Charging Quantum Batteries via Indefinite Causal Order: Theory and Experiment

Gaoyan Zhu,[1,*] Yuanbo Chen,[2,*] Yoshihiko Hasegawa,[2,†] and Peng Xue[1,‡]
[1]Beijing Computational Science Research Center, Beijing 100084, China
[2]Department of Information and Communication Engineering, Graduate School of Information Science and Technology, The University of Tokyo, Tokyo 113-8656, Japan

(Received 28 September 2022; revised 15 May 2023; accepted 25 October 2023; published 13 December 2023)

In the standard quantum theory, the causal order of occurrence between events is prescribed, and must be definite. This has been maintained in all conventional scenarios of operation for quantum batteries. In this study we take a step further to allow the charging of quantum batteries in an indefinite causal order (ICO). We propose a nonunitary dynamics-based charging protocol and experimentally investigate this using a photonic quantum switch. Our results demonstrate that both the amount of energy charged and the thermal efficiency can be boosted simultaneously. Moreover, we reveal a counterintuitive effect that a relatively less powerful charger guarantees a charged battery with more energy at a higher efficiency. Through investigation of different charger configurations, we find that ICO protocol can outperform the conventional protocols and gives rise to the anomalous inverse interaction effect. Our findings highlight a fundamental difference between the novelties arising from ICO and other coherently controlled processes, providing new insights into ICO and its potential applications.

DOI: 10.1103/PhysRevLett.131.240401

Introduction.—The counterintuitive behavior of a quantum system occupying coherently superposed states marks the departure of quantum physics from the classical realm. Notably, quantum superposition, and other nonclassical resources like entanglement are at the center of this surge of activity, as their existence lies at the root of a broad-spectrum impact on many fields, including quantum information, quantum optics, and quantum thermodynamics [1–7]. In the emerging field of quantum thermodynamics, the primary objective of quantum batteries research is to develop energy storage devices [8]. Quantum coherence is a crucial component in many quantum technologies and plays a significant role in quantum batteries [9–11]. Recent studies have focused on optimizing charging power [12,13], battery stability [14,15], and the role of nonclassical resources in this context [16–18].

On the other hand, contemporary physics has made significant efforts to reconcile two key pillars of our fundamental understanding of the universe: general relativity and quantum mechanics. Despite the absence of a full theory of quantum gravity, it is conjectured that modifications to the concept of causal structure should be incorporated into quantum gravity. In general relativity, dynamic causal structures exist, and introducing a quantum mechanical nature may result in exotic superpositions of the causal order of events. Processes where the causal order becomes nonseparable or indefinite have been discovered to exhibit the features of *indefinite causal order* [19]. Putting it simply, it has been found that the laws of quantum mechanics allow for quantum superposition of causal orders.

Conventionally, even within the context of quantum mechanics, events can only occur in a fixed causal order, meaning either "event A takes place before event B" or its

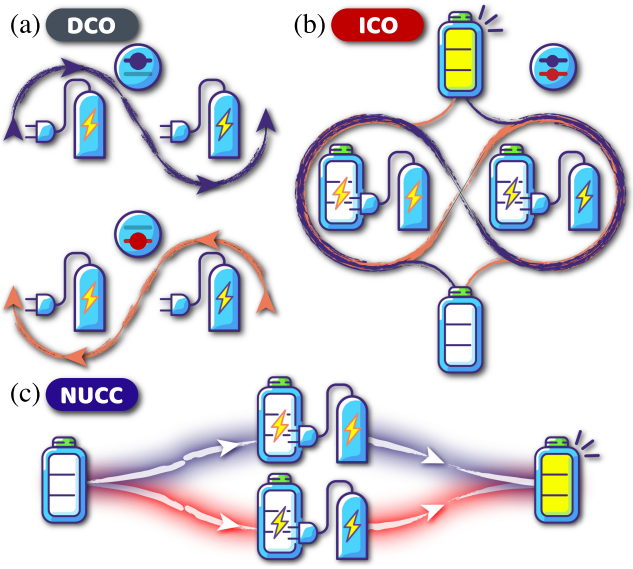

FIG. 1. Illustrations of the three scenarios. (a) DCO scenarios, where two chargers are sequentially arranged, resulting in either $\mathcal{C}_1 \circ \mathcal{C}_2$ (upper) or $\mathcal{C}_2 \circ \mathcal{C}_1$ (lower) configurations. (b) ICO charging realized by a QS that entangles two causal orders, allowing the causal order of operations on a quantum battery to be in a quantum superposition by preparing the order system in a superposition state. (c) NUCC protocol based on coherently controlling the path a battery takes, thereby achieving the effect of performing charging with $\mathcal{C}_1$ and $\mathcal{C}_2$ simultaneously.

reverse holds true. This conventional scenario is referred to as definite causal order (DCO). Recently, however, these constraints have been relaxed, allowing the two possibilities to be in superposition and leading to ICO. This exotic process can be realized using a quantum switch (QS) [20] to superimpose the causal order of events. A QS can be considered as a device that accepts two channels as inputs, and depending on the state of an order qubit, outputs a quantum superposition of channels in different causal orders. It has been demonstrated that QS is incompatible with the conventional assumption of fixed causal orders, and the inability of decomposing a QS into DCO processes has been explored [21].

Recent research on ICO has recognized it as a valuable resource, see Ref. [22] for a discussion in the thermodynamics context. Utilizing ICO offers numerous advantages in fields such as quantum communication [23–33], quantum computation [20,34–37], metrology [38–40], thermodynamics [41–47], and other quantum information tasks [48,49]. In quantum thermodynamics, incorporating ICO into thermalizing processes has led to the development of novel quantum refrigerators that have also been experimentally demonstrated [50]. Experimental investigations on ICO primarily rely on implementing a QS device [51–61].

In this Letter, through experimental realization of photonic QS and quantum simulation of QB, we present a novel scenario of ICO charging processes. To achieve this, we first construct a charging protocol that is based on nonunitary dynamics. Notably, the energy charged can be boosted to surpass population inversion, which is the best a conventional protocol can achieve, and the thermal efficiency, which is the ratio of ergotropy [62] to the corresponding work, also increases. Our result suggests that both quantities can break the bounds in the old scenario. We then demonstrate a strikingly counterintuitive effect: weaker coupling strength between the battery and ancillae results in more energy being charged, improving thermal efficiency. Through comparing charging processes in different scenarios, we finally address the essential and unique role ICO plays in outperforming conventional protocols and giving rise to the anomalous effect of weaker coupling with better performance.

Theoretical ideas.—Consider a situation where one has two chargers; classically, the order of operation of the two chargers $\mathcal{C}_1$ and $\mathcal{C}_2$ can be arranged so that the battery encounters $\mathcal{C}_1$ before $\mathcal{C}_2$, or vice versa. These are simply DCO scenarios. We can go a step further, as shown in Fig. 1(b), where the two chargers are arranged in a quantum superposition of two different configurations, i.e., a battery undergoes $\mathcal{C}_1 \circ \mathcal{C}_2$ and $\mathcal{C}_2 \circ \mathcal{C}_1$ simultaneously. This exotic scenario of ICO can be realized using a QS with the following mathematical description:

$$\mathbb{S}_{mn}(t) = |0\rangle\langle 0|^O \otimes K_2^n(t/2)K_1^m(t/2) + |1\rangle\langle 1|^O \otimes K_1^m(t/2)K_2^n(t/2), \quad (1)$$

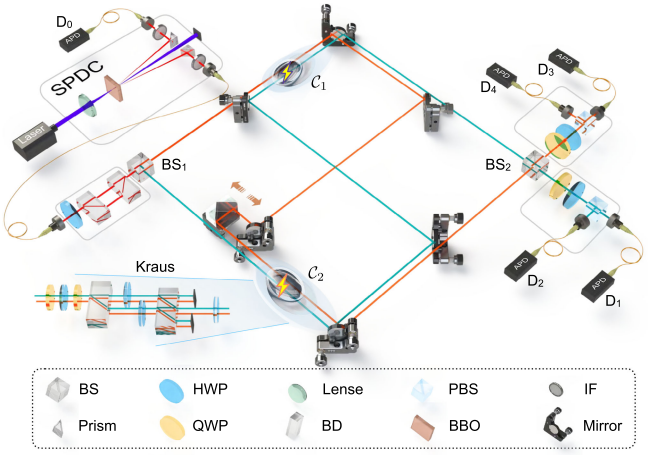

FIG. 2. Experimental setup, illustrating single photons produced through the type-I spontaneous parametric down-conversion (SPDC) process. A Mach-Zehnder interferometer structure realizes a QS, enabling the ICO charging process. The projecting measurements are carried out via a combination of QWP-HWP-PBS. Beam splitter (BS), half-wave plate (HWP), quarter-wave plate (QWP), beam displacer (BD), polarization beam splitter (PBS), β-barium borate (BBO), interference filter (IF), avalanche photodiode (APD).

where $K_{1(2)}^{m(n)}$ describe the action of $\mathcal{C}_{1(2)}$ in the Kraus form, with the superscript $m(n)$ counting the number of the Kraus operators, and $\{|0\rangle^O, |1\rangle^O\}$ forms the basis of the order qubit. As a third scenario, the nonunitary coherently controlled (NUCC) protocol, illustrated in Fig. 1(c), lies between the two we introduced. This protocol employs a control qubit that determines the target charger with which the battery interacts, enabling parallel charger application.

We use the following Hamiltonian as the model for our quantum battery:

$$\mathcal{H}_B = \frac{\omega}{2}(|e\rangle\langle e|^B - |g\rangle\langle g|^B), \quad (2)$$

where $\mathcal{H}_B$ is represented in terms of its energy spectrum, with $\{|e\rangle^B, |g\rangle^B\}$ being the energy basis, and $\omega > 0$. Our quantum battery can be defined by associating its *full* and *empty* states with $|e\rangle^B$ and $|g\rangle^B$.

Next, to specify the $K_{1(2)}^{m(n)}$ in Eq. (1), we consider the charging dynamics and represent the dynamical map describing the time evolution in the Kraus form. By adopting the nonunitary evolution-based protocol in [63], one can make several identical ancillae repeatedly interact with the battery to achieve charging (a unitary evolution-based one is presented in S3 of the Supplemental Material [64], where ICO also demonstrates its advantage). Here, we consider the ancillae Hamiltonian $\mathcal{H}_A = \omega/2(|e\rangle\langle e|^A - |g\rangle\langle g|^A)$, and assume that the interaction Hamiltonian is

$$\mathcal{H}_I = \kappa(\sigma_B^+ \otimes \sigma_A^+ + \sigma_B^- \otimes \sigma_A^-), \quad (3)$$

with $\sigma_{B(A)}^+ = |e\rangle\langle g|^{B(A)}$, $\sigma_{B(A)}^- = |g\rangle\langle e|^{B(A)}$, and $\kappa > 0$.

Let us assume that the initial state is mixed, such that $\rho_B = p|e\rangle\langle e|^B + (1-p)|g\rangle\langle g|^B$, where $0 \le p \le 1/2$. Next, we represent the dynamical map via $K^{m(n)}_{1(2)} \coloneqq K_{\mu\nu}(t) = \sqrt{P_\nu}\langle\mu|^A U(t)|\nu\rangle^A$, where $U(t) = \exp[-i\hbar t(\mathcal{H}_B + \mathcal{H}_A + \mathcal{H}_I)]$, $\mu,\nu \in \{e,g\}$, $\hbar = 1$ and assume that the ancilla is initialized to be $\rho_A = p|e\rangle\langle e|^A + (1-p)|g\rangle\langle g|^A$, so that $P_e = p$, $P_g = 1-p$. The map between $\mu\nu$ and $m(n)$ is, for example, $\mu\nu : ee \mapsto m(n) : 0$. There are four terms in the set of Kraus operators (see S1 in [64]): as an example,

$$K^0_{1(2)} \coloneqq K_{ee} = \sqrt{p}(\alpha|e\rangle\langle e|^B + |g\rangle\langle g|^B), \tag{4}$$

where $\alpha = \cos(\Theta t/2) - i(\omega/\Theta)\sin(\Theta t/2)$, and $\Theta = \sqrt{\kappa^2+\omega^2}$.

Under the current consideration, $\mathcal{C}_1$ and $\mathcal{C}_2$ are identical, see Ref. [64] for a discussion of asymmetrical chargers with distinct coupling strengths. The time evolution $\rho_{OB}(0) \mapsto \rho_{OB}(t)$ can be obtained via $\mathcal{SW}(\rho_{OB}) \coloneqq \sum_{mn} \mathbb{S}_{mn}(t)(\rho_O \otimes \rho_B)\mathbb{S}^\dagger_{mn}(t)$. Subsequently, we trace out the order qubit degrees of freedom after performing a projective measurement. Interesting outcomes arise in the $\rho^-_B(t)$ branch as it outperforms conventional scenarios and exhibits the anomalous effect, where $\rho^\pm_B(t) = \mathrm{Tr}_O[|\pm\rangle\langle\pm|^O \rho_{OB}(t)|\pm\rangle\langle\pm|^O]$ and $|\pm\rangle^O = (|0\rangle^O \pm |1\rangle^O)/\sqrt{2}$. Our protocol is of probabilistic nature, and the corresponding probability of success reads $P_{\mathrm{succ}}(t) = \mathrm{Tr}[\rho^-_B(t)]$.

In the following section, we characterize the ICO protocol from several perspectives, explaining in detail the intriguing aspects of the $\rho^-_B(t)$ branch. First, we examine the amount of energy in the battery. We introduce a quantity termed *population ratio*, which encodes information about the battery state, defined as $\mathcal{R} = \langle e|^B \rho |e\rangle^B / \langle g|^B \rho |g\rangle^B$.

It turns out that the population ratio can be boosted using our protocol. Meanwhile, one might wonder whether some form of sacrifice accompanies this advantage, in terms of, such as thermal efficiency. Interestingly, contrary to this naive expectation, we will demonstrate an enhancement in thermal efficiency. To proceed, we first define the variation in energy of the ancillae as heat, $\Delta Q = -(\mathrm{Tr}[\rho^-_{A_1A_2}\mathcal{H}_{A_1A_2}]/\mathrm{Tr}[\rho^-_{A_1A_2}] - \mathrm{Tr}[\rho_{A_1A_2}\mathcal{H}_{A_1A_2}])$. As the battery energy changes by $\Delta E = \mathrm{Tr}[\rho^-_B\mathcal{H}_B]/\mathrm{Tr}[\rho^-_B] - \mathrm{Tr}[\rho_B\mathcal{H}_B]$, by the first law [70], work is defined as $\Delta W = \mathrm{Tr}[\rho^-_{BA_1A_2}\mathcal{H}_{BA_1A_2}]/\mathrm{Tr}[\rho^-_{BA_1A_2}] - \mathrm{Tr}[\rho_{BA_1A_2}\mathcal{H}_{BA_1A_2}]$, where $A_{1(2)}$ denotes the first (second) ancilla. Another figure of merit we will use is ergotropy [62], defined as $\mathcal{E} = \max_U \mathrm{Tr}[(\rho - U\rho U^\dagger)\mathcal{H}]$. Thus, thermal efficiency is defined as $\eta = \mathcal{E}/\Delta W$.

Experiments.—As illustrated in Fig. 2, we experimentally realize the ICO charging process on a photonic system. In our implementation, the polarizations are encoded as battery qubits. The first beam splitter (BS_1 in Fig. 2) introduces spatial modes which are encoded as the order qubit, being initially $|+\rangle^O$. BS_2 projects it onto $|\pm\rangle^O$. The two charging processes appear in alternating order in the two arms of a Mach-Zehnder interferometer (MZI) [71–73]. Depending on the state of the order qubit ($|0\rangle^O$ or $|1\rangle^O$), the battery undergoes charging dynamics in the order of $\mathcal{C}_1 \circ \mathcal{C}_2$ or vice versa. Such a realization of photonic QS enables ICO charging processes.

The Kraus operators $K^{m(n)}_{1(2)}$ for the process $\mathcal{C}_{1(2)}$ can be realized [74–76] by the "Kraus" module as shown in Fig. 2. By concurrently deploying two modules for a pair of Kraus operators, K^m_1 and K^n_2, in the arms of the MZI, a QS in the form of Eq. (1) is realized (see Ref. [64]). The probabilities refer to parameters p and $1-p$ are applied in post-processing, by evaluating the ratios of the measurement outcomes from 16 separated experiments, thereby realizing the composite QS channel $\mathcal{SW}(\rho_{OB})$. For comparison, we also experimentally investigate the NUCC and DCO scenarios. The NUCC process is achieved by adjusting the position of $\mathcal{C}_{1(2)}$ for single-arm photon passage in the MZI. For the DCO process we remove the BSs of the MZI, allowing the battery to interact with $\mathcal{C}_1$ and $\mathcal{C}_2$ successively, with a process fidelity [67,68,77–79] above 99%, which is obtained by performing quantum process tomography [64].

Experimental results.—The population ratio of $\rho^-_B(t)$ is denoted as $\mathcal{R}^-(t)$. One naturally pays special attention to its maximum and minimum values. The two extrema, $\mathcal{R}^-_{\mathrm{min}}$ and $\mathcal{R}^-_{\mathrm{max}}$ are

$$\mathcal{R}^-_{\mathrm{min}} = \frac{1-p}{p}\frac{\omega^2(1-p)+\kappa^2p^2}{\omega^2p+\kappa^2(1-p)^2}, \tag{5a}$$

$$\mathcal{R}^-_{\mathrm{max}} = \left(\frac{1-p}{p}\right)^2. \tag{5b}$$

We also examine the population ratio $\mathcal{R}^-_*$, for which the corresponding success probability is maximized (see S1 in [64] for the derivation and expression for $\mathcal{R}^-_*$). Next, we examine what merits the ICO protocol compared to the DCO scenario. In terms of population ratio, the DCO protocol has the performance:

$$\mathcal{R}^{\mathrm{D}}_{\mathrm{max}} = \frac{\kappa^4(1-p)+2\kappa^2\omega^2(1-p)+\omega^4p}{\kappa^4p+2\kappa^2\omega^2p+\omega^4(1-p)}. \tag{6}$$

Let us consider two regimes to gain insight into the physics of Eq. (6): First, when $\kappa \ll \omega$, we find that $\mathcal{R}^{\mathrm{D}}_{\mathrm{max}} \approx p/(1-p)$, as does $\mathcal{R}^{\mathrm{D}}(t)$ [64]. Thus, $\mathcal{R}^{\mathrm{D}}(t)$ is flat, hence the battery almost remains unchanged. However, for $\kappa \gg \omega$, we have $\mathcal{R}^{\mathrm{D}}_{\mathrm{max}} \approx (1-p)/p$. Therefore, the best effect of the DCO protocol is population inversion, which is possible either by weakly coupling many copies of ancilla or with fewer ancillae but requires rather strong coupling. Figure 3(a) shows the dependence of $\mathcal{R}^-_*$, $\mathcal{R}^-_{\mathrm{max}}$, $\mathcal{R}^-_{\mathrm{min}}$, and $\mathcal{R}^{\mathrm{D}}_{\mathrm{max}}$ on κ/ω, on a logarithmic scale. Hence, a value of

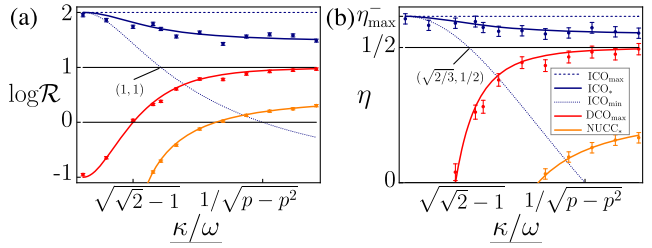

FIG. 3. Coupling strength dependence of performance for ICO charging protocol, its DCO, and NUCC counterparts. (a) Logarithm for population ratio $\log_{(1-p)/p}\mathcal{R}$ versus κ/ω. $\mathcal{R}_*^-$, $\mathcal{R}_{\max}^-$, $\mathcal{R}_{\min}^-$, $\mathcal{R}_{\max}^{\mathrm{D}}$, and $\mathcal{R}_*^{\mathrm{N},-}$ are shown by (blue) solid, dashed, dotted, red, and orange curves, respectively. The corresponding experimental results are shown by symbols. (b) Thermal efficiency η versus κ/ω, where the meaning of curves(dots) with distinct colors are similar to those in (a).

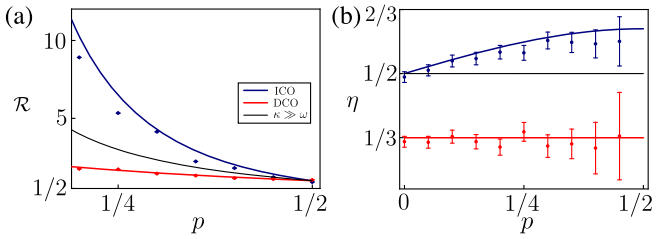

FIG. 4. Performance of protocol with fixed coupling strength ($\kappa/\omega = 1$). (a) Population ratio $\mathcal{R}$ versus parameter p of initial battery states. (b) Thermal efficiency η versus p. Experimental results and theoretical predictions are shown by dots and curves, respectively. Blue and red curves correspond to $\mathcal{R}_*^-$ (η_*^-) and $\mathcal{R}^{\mathrm{D}}$ (η^{D}), while gray curve represents $\mathcal{R}^{\mathrm{D}}$ (η^{D}) with coupling strength set to infinity.

$\log_{(1-p)/p}\mathcal{R}$ exceeding 1 is a signature of an advantage over the DCO protocol.

In the ICO protocol, an advantage in terms of population ratio is marked by the second power in Eq. (5b). Although coming with a vanishing probability, $\mathcal{R}_{\max}^-$ severs as a good estimation of the behavior of $\mathcal{R}^-(t)$ in the weak coupling regime, as explained later. Notice that unlike the maximum, Eq. (5a) depends on the system parameters and in fact may be worse than population inversion. As illustrated in Fig. 3(a), for $\kappa/\omega < 1$, $\mathcal{R}_{\min}^-$ breaks the DCO-scenario bound, implying that $\mathcal{R}^-(t)$ never falls out of the advantage region for any t. Taking $\mathcal{R}_{\max}^-$ as an estimation is typically useful when $\kappa \ll \omega$, because the difference between $\mathcal{R}_{\max}^-$ and $\mathcal{R}_{\min}^-$ vanishes if κ/ω becomes sufficiently small. Consequently, $\mathcal{R}^-(t)$ tends to be flat as its oscillation diminishes. Therefore, within the limit of $\kappa/\omega \to 0$, $\mathcal{R}^-(t) \approx (1-p)^2/p^2$ holds for all t. As a remark, the probability of $\mathcal{R}^-(t)$ vanishes if $\kappa/\omega = 0$ as the two charging processes reduce into two equivalent unitaries (see S2 in [64]), and hence our assumption of $\kappa > 0$. $\mathcal{R}_*^-$ is always located above the upper bound of the DCO protocol regardless of the initial state [Fig. 4(a)], or the coupling strength κ/ω [Fig. 3(a)].

Moreover, for a fixed ω, the relationship between $\mathcal{R}_*^-$ and κ is inverse; in other words, weaker coupling dynamics results in a higher $\mathcal{R}_*^-$, as shown in Fig. 3(a). Next, we compare the ICO protocol with the NUCC protocol. Interestingly, $\mathcal{R}_{\min}^-$ is equivalent to $\mathcal{R}_{\max}^{\mathrm{N},-}$ (see S2 in [64]) but with the replacement $\kappa/\omega \to (\kappa/\omega)^{-1}$. The theoretical predictions and experimental results of $\mathcal{R}_*^{\mathrm{N},-}$ (the NUCC counterpart of $\mathcal{R}_*^-$; see S2 in [64] for the derivation and expression) are plotted in Fig. 3(a) as orange lines and dots. This indicates that $\mathcal{R}_*^{\mathrm{N},-}$ is an increasing function of κ/ω, which is a feature shared by both the DCO and NUCC protocols. From this comparison, we conclude that the inverse relationship between κ/ω and performance can be uniquely attributed to ICO dynamics. This demonstrates an anomalous effect exclusive to ICO, unlike its role in other contexts. For instance, ICO is not the only resource that can activate communication abilities in noisy channels; similar effects can also be achieved by coherent control schemes [80]. This property offers some advantages for practical implementations and uncovers a previously unexplored inverse interaction effect. See S2 in [64] for an explanation of the anomalous effect.

From the perspective of thermal efficiency, $\eta^-(t)$ (see Ref. [64]) exhibits a behavior similar to $\mathcal{R}^-(t)$, where

$$\eta_{\min}^- = \frac{\omega^2 - \kappa^2 p(1-p)}{2\omega^2(1-p+p^2) + \kappa^2 p(1-p)}, \tag{7a}$$

$$\eta_{\max}^- = \frac{1}{2 - 2p(1-p)}. \tag{7b}$$

The thermal efficiency is meaningful when the charged battery is *not* passive [62], from which energy can be extracted unitarily. This condition is equivalent to the extent to which the population of $|e\rangle^B$ dominates, and requires $\kappa/\omega < 1/\sqrt{p-p^2}$. As shown in Ref. [63], the thermal efficiency of the DCO is upper bounded by $1/2$. However, for $\kappa/\omega < \sqrt{2/3}$, $\eta_{\min}^-$ exceeds $1/2$. The relationship between $\eta_{\min}^-$ and $\eta_{\max}^{\mathrm{N},-}$ of the NUCC scenario (see S2 in [64]) is the same as for population ratio. Furthermore, in the weak coupling limit $\eta^-(t) \approx \eta_{\max}^- = 2/3$. Similar to $\mathcal{R}_*^-$, the behavior of η_*^- (see Ref. [64]) is shown in Fig. 3(b).

For fixed coupling strengths, the performances evaluated for different initial states (p varying from 0 to 0.5) are shown in Fig. 4. The gray lines represent both the theoretical ICO-scenario lower bound and the DCO-scenario upper bound. The results clearly demonstrate that the ICO protocol can outperform the DCO protocol irrespective of the initial state.

Conclusion.—We proposed ICO quantum battery charging protocols and experimentally studied them in a photonic system. By comparing charging processes in three

scenarios, we demonstrated that ICO plays an essential role in outperforming conventional protocols, leading to the emergence of the counterintuitive effect. We expect that these novel findings of ICO will advance future quantum technologies.

This work has been supported by the National Natural Science Foundation of China (Grants No. 92265209 and No. 12025401). Y. H. acknowledges support by JSPS KAKENHI Grant No. JP22H03659. Y. C. acknowledges support by JST SPRING, Grant No. JPMJSP2108.

*These authors contributed equally to this work.
†hasegawa@biom.t.u-tokyo.ac.jp
‡gnep.eux@gmail.com

[1] T. D. Kieu, The second law, Maxwell's demon, and work derivable from quantum heat engines, Phys. Rev. Lett. **93**, 140403 (2004).
[2] H. T. Quan, P. Zhang, and C. P. Sun, Quantum heat engine with multilevel quantum systems, Phys. Rev. E **72**, 056110 (2005).
[3] M. Esposito, U. Harbola, and S. Mukamel, Nonequilibrium fluctuations, fluctuation theorems, and counting statistics in quantum systems, Rev. Mod. Phys. **81**, 1665 (2009).
[4] M. Campisi, P. Hänggi, and P. Talkner, Colloquium: Quantum fluctuation relations: Foundations and applications, Rev. Mod. Phys. **83**, 771 (2011).
[5] J. P. S. Peterson, T. B. Batalhão, M. Herrera, A. M. Souza, R. S. Sarthour, I. S. Oliveira, and R. M. Serra, Experimental characterization of a spin quantum heat engine, Phys. Rev. Lett. **123**, 240601 (2019).
[6] P. A. Camati, J. F. G. Santos, and R. M. Serra, Coherence effects in the performance of the quantum Otto heat engine, Phys. Rev. A **99**, 062103 (2019).
[7] P. A. Camati, J. F. G. Santos, and R. M. Serra, Employing non-Markovian effects to improve the performance of a quantum Otto refrigerator, Phys. Rev. A **102**, 012217 (2020).
[8] R. Alicki and M. Fannes, Entanglement boost for extractable work from ensembles of quantum batteries, Phys. Rev. E **87**, 042123 (2013).
[9] J. Monsel, M. Fellous-Asiani, B. Huard, and A. Auffèves, The energetic cost of work extraction, Phys. Rev. Lett. **124**, 130601 (2020).
[10] D. Rossini, G. M. Andolina, D. Rosa, M. Carrega, and M. Polini, Quantum advantage in the charging process of Sachdev-Ye-Kitaev batteries, Phys. Rev. Lett. **125**, 236402 (2020).
[11] L. P. García-Pintos, A. Hamma, and A. del Campo, Fluctuations in extractable work bound the charging power of quantum batteries, Phys. Rev. Lett. **125**, 040601 (2020).
[12] F. Campaioli, F. A. Pollock, F. C. Binder, L. Céleri, J. Goold, S. Vinjanampathy, and K. Modi, Enhancing the charging power of quantum batteries, Phys. Rev. Lett. **118**, 150601 (2017).
[13] D. Ferraro, M. Campisi, G. M. Andolina, V. Pellegrini, and M. Polini, High-power collective charging of a solid-state quantum battery, Phys. Rev. Lett. **120**, 117702 (2018).
[14] F. Pirmoradian and K. Mølmer, Aging of a quantum battery, Phys. Rev. A **100**, 043833 (2019).
[15] J. Q. Quach and W. J. Munro, Using dark states to charge and stabilize open quantum batteries, Phys. Rev. Appl. **14**, 024092 (2020).
[16] S. Julià-Farré, T. Salamon, A. Riera, M. N. Bera, and M. Lewenstein, Bounds on the capacity and power of quantum batteries, Phys. Rev. Res. **2**, 023113 (2020).
[17] G. M. Andolina, M. Keck, A. Mari, M. Campisi, V. Giovannetti, and M. Polini, Extractable work, the role of correlations, and asymptotic freedom in quantum batteries, Phys. Rev. Lett. **122**, 047702 (2019).
[18] K. V. Hovhannisyan, M. Perarnau-Llobet, M. Huber, and A. Acín, Entanglement generation is not necessary for optimal work extraction, Phys. Rev. Lett. **111**, 240401 (2013).
[19] O. Oreshkov, F. Costa, and Č. Brukner, Quantum correlations with no causal order, Nat. Commun. **3**, 1092 (2012).
[20] G. Chiribella, G. M. D'Ariano, P. Perinotti, and B. Valiron, Quantum computations without definite causal structure, Phys. Rev. A **88**, 022318 (2013).
[21] O. Oreshkov and C. Giarmatzi, Causal and causally separable processes, New J. Phys. **18**, 093020 (2016).
[22] M. Capela, H. Verma, F. Costa, and L. C. Céleri, Reassessing thermodynamic advantage from indefinite causal order, Phys. Rev. A **107**, 062208 (2023).
[23] G. Chiribella, Perfect discrimination of no-signalling channels via quantum superposition of causal structures, Phys. Rev. A **86**, 040301(R) (2012).
[24] A. Feix, M. Araújo, and Č. Brukner, Quantum superposition of the order of parties as a communication resource, Phys. Rev. A **92**, 052326 (2015).
[25] P. A. Guérin, A. Feix, M. Araújo, and Č. Brukner, Exponential communication complexity advantage from quantum superposition of the direction of communication, Phys. Rev. Lett. **117**, 100502 (2016).
[26] F. Del Santo and B. Dakić, Two-way communication with a single quantum particle, Phys. Rev. Lett. **120**, 060503 (2018).
[27] D. Ebler, S. Salek, and G. Chiribella, Enhanced communication with the assistance of indefinite causal order, Phys. Rev. Lett. **120**, 120502 (2018).
[28] G. Chiribella and H. Kristjánsson, Quantum Shannon theory with superpositions of trajectories, Proc. R. Soc. A **475**, 20180903 (2019).
[29] L. M. Procopio, F. Delgado, M. Enríquez, N. Belabas, and J. A. Levenson, Communication enhancement through quantum coherent control of N channels in an indefinite causal-order scenario, Entropy **21**, 1012 (2019).
[30] N. Loizeau and A. Grinbaum, Channel capacity enhancement with indefinite causal order, Phys. Rev. A **101**, 012340 (2020).
[31] G. Chiribella, M. Banik, S. S. Bhattacharya, T. Guha, M. Alimuddin, A. Roy, S. Saha, S. Agrawal, and G. Kar, Indefinite causal order enables perfect quantum communication with zero capacity channels, New J. Phys. **23**, 033039 (2021).
[32] G. Chiribella, M. Wilson, and H. F. Chau, Quantum and classical data transmission through completely depolarizing

channels in a superposition of cyclic orders, Phys. Rev. Lett. **127**, 190502 (2021).
[33] H. Kristjánsson, W. Mao, and G. Chiribella, Witnessing latent time correlations with a single quantum particle, Phys. Rev. Res. **3**, 043147 (2021).
[34] T. Colnaghi, G. M. D'Ariano, S. Facchini, and P. Perinotti, Quantum computation with programmable connections between gates, Phys. Lett. A **376**, 2940 (2012).
[35] T. Morimae, Acausal measurement-based quantum computing, Phys. Rev. A **90**, 010101(R) (2014).
[36] M. Araújo, F. Costa, and Č. Brukner, Computational advantage from quantum-controlled ordering of gates, Phys. Rev. Lett. **113**, 250402 (2014).
[37] M. J. Renner and Č. Brukner, Computational advantage from a quantum superposition of qubit gate orders, Phys. Rev. Lett. **128**, 230503 (2022).
[38] M. Frey, Indefinite causal order aids quantum depolarizing channel identification, Quantum Inf. Process. **18**, 96 (2019).
[39] X. Zhao, Y. Yang, and G. Chiribella, Quantum metrology with indefinite causal order, Phys. Rev. Lett. **124**, 190503 (2020).
[40] F. Chapeau-Blondeau, Noisy quantum metrology with the assistance of indefinite causal order, Phys. Rev. A **103**, 032615 (2021).
[41] T. Guha, M. Alimuddin, and P. Parashar, Thermodynamic advancement in the causally inseparable occurrence of thermal maps, Phys. Rev. A **102**, 032215 (2020).
[42] D. Felce and V. Vedral, Quantum refrigeration with indefinite causal order, Phys. Rev. Lett. **125**, 070603 (2020).
[43] K. Simonov, G. Francica, G. Guarnieri, and M. Paternostro, Work extraction from coherently activated maps via quantum switch, Phys. Rev. A **105**, 032217 (2022).
[44] K. Simonov, Indefinite causality in quantum mechanics and its thermodynamic applications, J. Phys. Conf. Ser. **2533**, 012039 (2023).
[45] P. R. Dieguez, V. F. Lisboa, and R. M. Serra, Thermal devices powered by generalized measurements with indefinite causal order, Phys. Rev. A **107**, 012423 (2023).
[46] G. Francica, Causal games of work extraction with indefinite causal order, Phys. Rev. A **106**, 042214 (2022).
[47] J. Zhao and Y. Xu, Influence of an indefinite causal order on an Otto heat engine, Commun. Theor. Phys. **74**, 025601 (2022).
[48] M. T. Quintino, Q. Dong, A. Shimbo, A. Soeda, and M. Murao, Reversing unknown quantum transformations: Universal quantum circuit for inverting general unitary operations, Phys. Rev. Lett. **123**, 210502 (2019).
[49] J. Bavaresco, M. Murao, and M. T. Quintino, Strict hierarchy between parallel, sequential, and indefinite-causal-order strategies for channel discrimination, Phys. Rev. Lett. **127**, 200504 (2021).
[50] X. Nie, X. Zhu, K. Huang, K. Tang, X. Long, Z. Lin, Y. Tian, C. Qiu, C. Xi, X. Yang, J. Li, Y. Dong, T. Xin, and D. Lu, Experimental realization of a quantum refrigerator driven by indefinite causal orders, Phys. Rev. Lett. **129**, 100603 (2022).
[51] L. M. Procopio, A. Moqanaki, M. Araújo, F. Costa, I. Alonso Calafell, E. G. Dowd, D. R. Hamel, L. A. Rozema, Č. Brukner, and P. Walther, Experimental superposition of orders of quantum gates, Nat. Commun. **6**, 7913 (2015).
[52] G. Rubino, L. A. Rozema, A. Feix, M. Araújo, J. M. Zeuner, L. M. Procopio, Č. Brukner, and P. Walther, Experimental verification of an indefinite causal order, Sci. Adv. **3**, e1602589 (2017).
[53] K. Goswami, C. Giarmatzi, M. Kewming, F. Costa, C. Branciard, J. Romero, and A. G. White, Indefinite causal order in a quantum switch, Phys. Rev. Lett. **121**, 090503 (2018).
[54] K. Wei, N. Tischler, S.-R. Zhao, Y.-H. Li, J. M. Arrazola, Y. Liu, W. Zhang, H. Li, L. You, Z. Wang, Y.-A. Chen, B. C. Sanders, Q. Zhang, G. J. Pryde, F. Xu, and J.-W. Pan, Experimental quantum switching for exponentially superior quantum communication complexity, Phys. Rev. Lett. **122**, 120504 (2019).
[55] F. Massa, A. Moqanaki, Ä. Baumeler, F. Del Santo, J. A. Kettlewell, B. Dakić, and P. Walther, Experimental two-way communication with one photon, Adv. Quantum Technol. **2**, 1900050 (2019).
[56] Y. Guo, X.-M. Hu, Z.-B. Hou, H. Cao, J.-M. Cui, B.-H. Liu, Y.-F. Huang, C.-F. Li, G.-C. Guo, and G. Chiribella, Experimental transmission of quantum information using a superposition of causal orders, Phys. Rev. Lett. **124**, 030502 (2020).
[57] K. Goswami, Y. Cao, G. A. Paz-Silva, J. Romero, and A. G. White, Increasing communication capacity via superposition of order, Phys. Rev. Res. **2**, 033292 (2020).
[58] G. Rubino, L. A. Rozema, D. Ebler, H. Kristjánsson, S. Salek, P. Allard Guérin, A. A. Abbott, C. Branciard, Č. Brukner, G. Chiribella, and P. Walther, Experimental quantum communication enhancement by superposing trajectories, Phys. Rev. Res. **3**, 013093 (2021).
[59] M. M. Taddei, J. Cariñe, D. Martínez, T. García, N. Guerrero, A. A. Abbott, M. Araújo, C. Branciard, E. S. Gómez, S. P. Walborn, L. Aolita, and G. Lima, Computational advantage from the quantum superposition of multiple temporal orders of photonic gates, PRX Quantum **2**, 010320 (2021).
[60] Y. Chen and Y. Hasegawa, EPR pairs from indefinite causal order, arXiv:2112.03233.
[61] G. Rubino, L. A. Rozema, F. Massa, M. Araújo, M. Zych, Č. Brukner, and P. Walther, Experimental entanglement of temporal order, Quantum **6**, 621 (2022).
[62] A. E. Allahverdyan, R. Balian, and T. M. Nieuwenhuizen, Maximal work extraction from finite quantum systems, Europhys. Lett. **67**, 565 (2004).
[63] F. Barra, Dissipative charging of a quantum battery, Phys. Rev. Lett. **122**, 210601 (2019).
[64] See Supplemental Material at http://link.aps.org/supplemental/10.1103/PhysRevLett.131.240401 for details on experimental methods, calculation of population ratio and thermodynamic quantities, comparison with a nonunitary protocol based on coherently controlled processes, and the ICO unitary protocol, which includes Refs. [65–69].
[65] D. F. V. James, P. G. Kwiat, W. J. Munro, and A. G. White, Measurement of qubits, Phys. Rev. A **64**, 052312 (2001).
[66] R. Jozsa, Fidelity for mixed quantum states, J. Mod. Opt. **41**, 2315 (1994).

[67] X. Wang, C.-S. Yu, and X. Yi, An alternative quantum fidelity for mixed states of qudits, Phys. Lett. A **373**, 58 (2008).

[68] J. Zhang, A. M. Souza, F. D. Brandao, and D. Suter, Protected quantum computing: Interleaving gate operations with dynamical decoupling sequences, Phys. Rev. Lett. **112**, 050502 (2014).

[69] C. Branciard, Witnesses of causal nonseparability: An introduction and a few case studies, Sci. Rep. **6**, 26018 (2016).

[70] P. Strasberg, G. Schaller, T. Brandes, and M. Esposito, Quantum and information thermodynamics: A unifying framework based on repeated interactions, Phys. Rev. X **7**, 021003 (2017).

[71] L. Xiao, T. Deng, K. Wang, G. Zhu, Z. Wang, W. Yi, and P. Xue, Non-Hermitian bulk–boundary correspondence in quantum dynamics, Nat. Phys. **16**, 761 (2020).

[72] K. Wang, L. Xiao, J. C. Budich, W. Yi, and P. Xue, Simulating exceptional non-Hermitian metals with single-photon interferometry, Phys. Rev. Lett. **127**, 026404 (2021).

[73] K. Wang, X. Qiu, L. Xiao, X. Zhan, Z. Bian, W. Yi, and P. Xue, Simulating dynamic quantum phase transitions in photonic quantum walks, Phys. Rev. Lett. **122**, 020501 (2019).

[74] A. Cuevas, M. Proietti, M. A. Ciampini, S. Duranti, P. Mataloni, M. F. Sacchi, and C. Macchiavello, Experimental detection of quantum channel capacities, Phys. Rev. Lett. **119**, 100502 (2017).

[75] N. Tischler, C. Rockstuhl, and K. Słowik, Quantum optical realization of arbitrary linear transformations allowing for loss and gain, Phys. Rev. X **8**, 021017 (2018).

[76] K. Wang, X. Wang, X. Zhan, Z. Bian, J. Li, B. C. Sanders, and P. Xue, Entanglement-enhanced quantum metrology in a noisy environment, Phys. Rev. A **97**, 042112 (2018).

[77] M. F. Sacchi, Maximum-likelihood reconstruction of completely positive maps, Phys. Rev. A **63**, 054104 (2001).

[78] G. M. D'Ariano and P. Lo Presti, Quantum tomography for measuring experimentally the matrix elements of an arbitrary quantum operation, Phys. Rev. Lett. **86**, 4195 (2001).

[79] I. L. Chuang and M. A. Nielsen, Prescription for experimental determination of the dynamics of a quantum black box, J. Mod. Opt. **44**, 2455 (1997).

[80] A. A. Abbott, J. Wechs, D. Horsman, M. Mhalla, and C. Branciard, Communication through coherent control of quantum channels, Quantum **4**, 333 (2020).